

CHAPTER 6: METAL CATHODES

TRIVENI RAO

Brookhaven National Laboratory

Upton, NY 11973

JOHN SMEDLEY

Brookhaven National Laboratory

Upton, NY 11973

Keywords

Photocathode, Quantum Efficiency, Metal Cathode, Copper Cathode, Magnesium Cathode, Lead Cathode, Niobium Cathode, Three-Step Model, Theoretical Calculation of Quantum Efficiency, Experimental Measurement of Quantum Efficiency, Intrinsic Emittance, Laser cleaning, Hydrogen Cleaning, Cathode Polishing, Arc Deposition, Friction Welding, Cathode Plug, Choke Joint

Abstract

A number of low to medium current, high brightness injectors use metal photocathodes for electron emission. The theory is developed in Chapter 5 and is applied in this chapter to calculate the QE of copper and lead, as examples. It has been shown experimentally that the QE of the as received cathode material can be improved significantly by appropriate processing. We describe in detail different cleaning techniques adopted in operational facilities, such as laser cleaning and ion cleaning. Incorporating the cathode in the injector is a non-trivial problem, especially if it is a dissimilar metal placed in a high field environment. We describe a number of techniques used including *in-situ* application, embedding the cathode in a plug, a flange, and a choke joint assembly and provide examples for each.

6.1 INTRODUCTION

Metal cathodes often are the default choice for low average current photoinjector applications, as they are easy to prepare and have a long operational lifetime with minimal vacuum requirements. They are prompt emitters, with an emission time of tens of femtoseconds; their high work functions lead to low dark currents even in high electric fields. Over the past two decades, copper and magnesium cathodes have been used [6.1]–[6.4] in high-brightness, low average current, low repetition rate normal conducting RF (NCRF) injectors. Table 6.1 lists some performance parameters using these photocathodes. [6.5]

Much of the recent interest [6.6]–[6.8] has centered on increasing both the repetition rate and the average current for several applications. Superconducting RF (SCRf) injectors were proposed for them so they may maintain a relatively high accelerating gradient and very low resistive loss of the RF power. Niobium, a natural choice for cavity material, has been tested [6.9]. The quantum efficiency (QE) measured [6.10] on Nb witness samples indicate average currents around 50 μA are possible with today's commercial lasers. Another metal cathode candidate is lead, a Type I superconductor, commonly used in ion accelerators. QE measurements with lead witness samples indicate that its QE can be as high as 0.5% for 6.4 eV photons. Hence, for attaining a higher average current, a lead cathode was tested both in a DC set-up with witness pieces [6.11] and in a 1.3 GHz SCRf gun [6.12].

One major drawback of the metal cathodes is their high work function, typically in the 4-5 eV regime that requires the operating wavelength of the driving laser to be in the UV range. Even at this large photon energy, the QE is only a fraction of a percent. The combination of these two factors and the power levels achievable with existing commercial lasers restrict their use primarily to intermediate average current applications. Furthermore, as explained in Chapter 5, of all the photo-excited electrons, only those that did not undergo inelastic electron-electron collision have enough energy to overcome the work function, and are emitted. Thus, assuming an isotropic velocity distribution for the electrons (for example, a polycrystalline cathode with no preferential emission directions), the maximum energy of the emitted electrons is $\sim(h\nu - \phi)$, where $h\nu$ is the photon energy, and ϕ is the work function. As the QE scales roughly as $(h\nu - \phi)^2$ and intrinsic emittance as $(h\nu - \phi)^{1/2}$, there is a tradeoff between high QE and low emittance for these cathodes.

Facility	Cathode Material	Preparation	Laser Wavelength	Charge	Pulse Duration	Repetition Rate	Lifetime
LCLS	Copper	H ₂ Ion Bombardment\ Laser Ablation	253, 255 nm	Up to 1 nC	0.7-3.7 ps	120 Hz	2 yr
BNL-ATF	Copper	Laser Ablation	256 nm	Up to 1 nC	7 ps	Up to 6 Hz	> 5 yrs
BNL-LEAF	Magnesium	Laser Ablation	266 nm	8 nC	5 ps	10 Hz	18 months
UCLA	Copper with MgF ₂ Coating	Laser Ablation	266, 800 nm	10 pc	< 1 ps	5 Hz	> 1 yr
INFN: FERMI	Copper	Ozone Cleaning	262 nm	250 pC	6 pc	10 Hz	3 months

Table 6.1. Facilities using metal photocathodes and their performance [6.5].

In this chapter, we discuss the experimental measurements and theoretical calculations of the QE, its enhancement with surface treatment, the impact of the surface treatment on the emittance, and the incorporation of the cathodes in RF cavities.

6.2 EXPERIMENTAL MEASUREMENTS AND THEORETICAL CALCULATIONS OF THE QE

The QE of several metals have been measured in laboratory settings [6.13] and the QE of Mg, Cu, Nb, and Pb was measured in RF guns/injectors; the values are listed in Table 6.2. We will describe here the theoretical calculations and the QE measurements for Pb and Cu.

Metal @ Electric Field	Wavelength [nm]	QE [%]
Copper @ 100 MV m ⁻¹	266	0.014
Magnesium @ 100 MV m ⁻¹	266	0.62
Niobium @ 2 MV m ⁻¹	266	~0.001
Lead @ 2 MV m ⁻¹	248	0.016

Table 6.2. Quantum efficiency of selected metals measured in these respective electric fields in RF guns.

As described in Chapter 5, three independent steps, developed by Spicer, describe the photoemission process to the first order [6.14]. The first step is the transmission of an incident photon of energy, $h\nu$, into

the material, then the absorption of this photon by an electron and its excitation from an energy state $(E - h\nu)$ to an energy state E . The second step is the transit of this electron to the surface; and the third is its escape from the cathode's surface. Explicit expressions for the probability of each of the steps were derived in Chapter 5. Here, we describe the methodology for calculating the QE of lead from these expressions. For this calculation, we made the following assumptions:

- The sample is sufficiently thick to absorb all the transmitted photons.
- The material is polycrystalline non-crystalline, and hence, only energy conservation is imposed in the excitation process.
- The excitation process is isotropic.
- Electron-phonon (e-p) collision is nearly elastic, and so can be ignored.
- Electron-electron scattering will result in both the electrons involved having insufficient energy to escape the material (so they are effectively lost).

6.2.1 Step 1

Two factors dictate the probability of the absorption of a photon of energy, $h\nu$: The transmission coefficient of the metal at $h\nu$, and the number of accessible initial- and final-states. The transmission coefficient is calculated from the optical constants of Pb. The accessible states are the product of the density of states (DOS) and the Fermi-Dirac distribution. To the first approximation, we can use the Fermi-Dirac distribution function at zero temperature, with all the states below Fermi energy filled, and all those above it empty. The simplified form of this probability is

$$P(E, h\nu) = (1 - R(\nu)) \frac{N(E)N(E - h\nu)}{E_f + h\nu \int_{E_f} dE' N(E')N(E' - h\nu)} \quad (6.1)$$

where $R(\nu)$ is the reflectivity of the cathode at $h\nu$. This probability calculated for lead is shown in Figure 6.1, and databases [6.15] such as the Naval Research Laboratory's (NRL) structures database are available to reference the DOS for a large variety of elements and compounds. The optical constants and work function are from [6.16], [6.17].

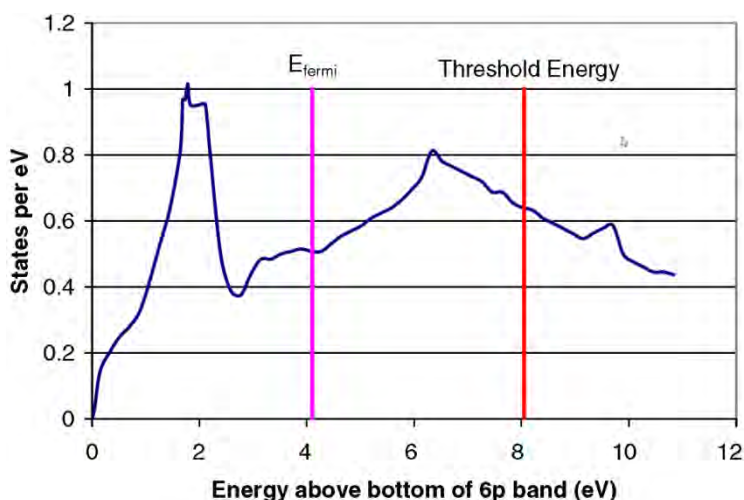


Figure 6.1. Calculated Density of Electronic States for lead, with E_{fermi} referenced to the bottom of the filled 6p band where the vertical axis is the number of states per electron volt within the material. [Reprinted figure with permission from [6.11]. Copyright 2008 by the American Physical Society]

6.2.2 Step 2

The electrons with energy E are generated in lead at depths dictated by the photon's absorption length. During their transit from the point of excitation to the surface, the electrons undergo e-e and e-p scattering; the latter primarily changes the electrons' trajectory. Since we assumed that the excitation was isotropic, we can neglect the impact of e-p collision. For the photon energies under consideration here, hot electrons undergoing inelastic e-e scattering will not be sufficiently energetic to overcome the work function. Hence, the fraction of the excited electrons that reach the surface is

$$F_{e-e}(E, h\nu) = C \frac{\lambda_e(E)/\lambda_{ph}(\nu)}{1 + (\lambda_e(E)/\lambda_{ph}(\nu))} \quad (6.2)$$

where $\lambda_{opt} = \lambda (4\pi k)^{-1}$, k is the imaginary part of the complex index of refraction, and λ_{e-e} is the electron mean free path for e-e scattering. C is the form factor that takes into account that the electron's trajectory may not be normal to the surface. For most of the near threshold cases, the escape cone is narrow enough that C can be taken to be unity. The absorption depth is calculated using optical constants. The lifetime of the electrons is derived from first principles, assuming a free electron DOS and its mean free path are given by the product of the lifetime by the electron velocity.

6.2.3 Step 3

To escape the surface, the momentum of the electron normal to the surface, k_{\perp} , must satisfy the condition

$$\frac{\hbar k_{\perp}^2}{2m} > E_T \quad (6.3)$$

wherein $E_T = E_f + \phi$. In the presence of an accelerating field E_{acc} , the threshold energy, E_T , is reduced by $\phi_{Schottky}$ [eV] = $3.7947 \times 10^{-5} \sqrt{E_{acc} [\text{V m}^{-1}]}$ due to the Schottky effect. The probability that an excited electron of energy E escapes the surface is given by

$$D(E) = \frac{1}{2} \left(1 - \sqrt{\frac{E_T}{E - E_f}} \right) \quad (6.4)$$

The quantum efficiency is

$$QE(h\nu) = \int_{E_f + \phi_{eff}}^{E_f + h\nu} dE P(E, h\nu) F_{e-e}(E, h\nu) D(E) \quad (6.5)$$

where $D(E)$ is the fraction of the electrons with sufficient longitudinal momentum to overcome the work function. Figure 6.2 shows the calculated quantum efficiency of lead as a function of photon energy using 3.95 eV for ϕ .

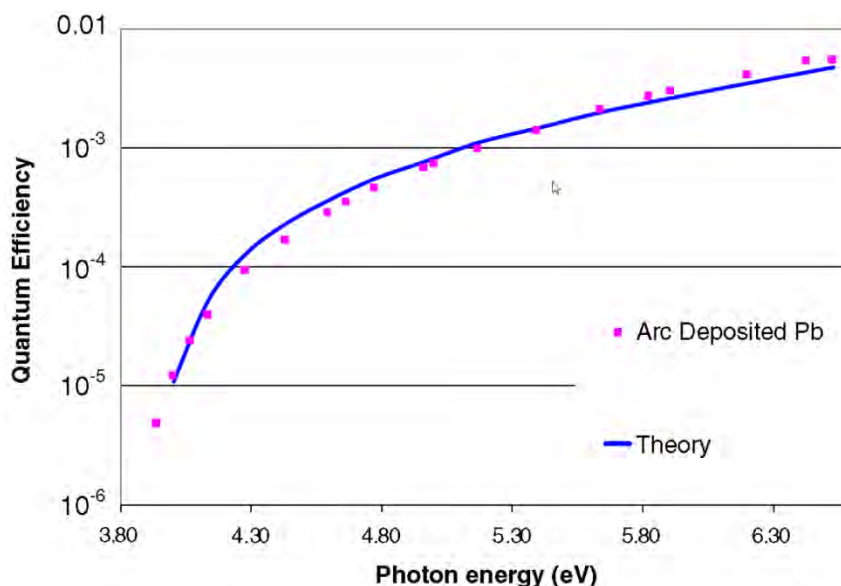


Figure 6.2. Experimental- (■) and theoretical- (—) spectral dependence of QE on an arc-deposited lead witness sample. [Reprinted figure with permission from [6.11]. Copyright 2008 by the American Physical Society]

QE is measured for an arc-deposited lead cathode in the laboratory with a mesh anode held in parallel to the cathode in an evacuated cube. The anode is held at a positive bias and a picoammeter measures the current leaving the cathode. A deuterium light source is fiber-coupled to a monochromator with a 300 μm exit slit. The desired wavelength λ is selected on the monochromator. The output bandwidth is 2 nm, measured with an Ocean Optics HR2000 spectrometer. A fused silica lens focuses the light on the cathode through a vacuum window and the anode mesh. We measure, with a power meter, the output of the monochromator for each wavelength before and after each current measurement at a point after the lens, but before the vacuum window. The optical transmission of the vacuum window and the mesh are calibrated separately for each wavelength. Typical values for optical power P (in a 2 nm band) are 10-100 nW, and those for current I are 0.1-10 pA. For each wavelength, the QE is calculated *via*

$$\text{QE} = \frac{I h \nu}{P}; \text{ where } \nu = \frac{c}{\lambda} \quad (6.6)$$

Figure 6.2 compares the theoretical calculation and experimental measurements. Other researchers made similar calculations for copper [6.18]. The calculations for copper can be simplified greatly. For near-threshold emission, copper's DOS is nearly constant from 2 eV below the Fermi level up to the vacuum level; the Fermi-Dirac distribution can be assumed to be a step function. The probability expressions are simplified to generate an analytical expression for the energy distribution as well as the QE.

6.3 INTRINSIC EMITTANCE OF METAL CATHODES

The intrinsic emittance of the electrons at the surface of the cathode can be written as Equ. 5.30. As can be seen from the equation, the intrinsic emittance of the electrons from a cathode is dictated by the laser spot size, the photon energy and the applied field. The intrinsic emittance can be lowered by reducing the laser spot size and matching the laser photon energy closely to the effective work function of the cathode. Intrinsic emittance of 0.41 mm mrad mm^{-1} and 0.68 mm mrad mm^{-1} have been experimentally measured for hand polished polycrystalline copper irradiated by 282 nm and 262 nm laser, respectively [6.19]. However, one should keep in mind that matching the laser photon energy to the work function leads to a reduction in the quantum efficiency as well. The QE measured for this sample is 1×10^{-5} at 262 nm and 5×10^{-6} at 282 nm.

As mentioned in Chapter 5, the surface roughness can alter the intrinsic emittance as well, especially in the presence of an applied field. Dependence of QE and the thermal emittance of copper cathode in a RF gun has been measured by [6.20].

6.4 CATHODE PREPARATION TECHNIQUES

Since most metals, as received from a vendor, have surface contaminants, their QE is significantly lower than that predicted for a pure sample. The QE however can be improved by surface processing. A number of techniques have been tested and a few established ones are described below

6.4.1 Ex-Situ Preparation

6.4.1.1 Surface Preparation of Copper- and Magnesium-Cathodes

The surface preparation described here, used in conjunction with laser cleaning, increases the electron yield by two to three orders-of-magnitude. Although we have used this procedure in a laboratory setting on several metal cathodes [6.13], it was tested in the RF injector only on copper- and magnesium-cathodes since these are the preferred ones for the applications. Comparison of the cathode's performance after using polishing products from different vendors revealed that the process is product-specific. We recommend using the ones specified in the process for optimum results.

1. Select high-purity bulk material (*e.g.*, high-purity, oxygen-free copper (OFC), high-purity Mg rod) as the source for the cathode.
2. After machining to the required dimensions, remove any fine scratches and ensure surface flatness using the following procedure:
 - a. Mount three identical cathodes on a face plate (one intended cathode and two witness cathodes) in a circle at 120° apart. Dissimilar metals cross-contaminate the cathode's surface. Dissimilar sizes may degrade surface flatness.
 - b. Adjust the three cathodes so that they are parallel to the face plate to within 0.025 mm.
 - c. Remove surface scratches on the cathode by polishing its surface with Buehler Microcut 600 grit paper and then with Buehler Metadi fluid polishing extender. Using other polishing products did not reproducibly increase electron yield by two to three orders-of-magnitude.
3. The surface preparation is completed using a double platen, Buehler Ecomet 5 polishing grinder with Automet 2 power head, and a Buehler Mastertex polishing cloth. One of the platens and associated workstation is reserved for the final polishing with a 1-micron diamond polishing compound, and hence, is kept covered to avoid contamination, while the other station was used to polish the cathode successively with 9-micron- and 6-micron-polishing compounds. The polishing cloth is attached to the platen rotating at 120 RPM. The Buehler Metadi 9-micron suspension is sprayed on the polishing cloth, soaking it so that the liquid pools in the cloth. The Automet is set for a polishing time of 90 sec at a pressure of 3 lbs. The cathode in the chuck fixture is attached to the Automet and lowered on to the platens.

If the cathode's surface is too large for faceplate to support, the positions of the cathode and the polishing cloth can be interchanged. If the cathode is integrated into a flange that prevents its being polished in the polishing machine, it can be mounted on a lathe and the cathode polished by holding the polishing cloth in front of it. In this case, the lathe should not rotate above 300 RPM.

4. Rinse the cathode and the fixture with hexane. Hexane was chosen as the cleanser because it does not contain oxygen and effectively removes the suspension residue from the cathode surface.
5. Repeat the polishing process with the 6-micron diamond suspension.
6. Switch over to the other head and workstation.

7. Repeat the polishing with the 1-micron diamond suspension, but reduce the polishing time to 60 sec; then inspect the surface and repeat if necessary. Over-polishing may introduce peeling, engendering a surface texture resembling an orange peel, observable even to the naked eye.
8. Rinse the cathode completely with hexane.
9. Remove the cathode quickly from the fixture and immerse it in a hexane bath in a beaker.
10. Place the beaker in an ultrasonic cleaner for 20 min to remove any embedded polishing material. Ensure that the temperature of the hexane does not rise above room temperature during this process.
11. Remove the cathode from hexane and dry the surface with high purity nitrogen at 60 psig.
12. Transfer the cathode to the vacuum system and start pumping down. The time lapse between drying with nitrogen and the pump down should be minimized (< 2 min).

The cathode is now ready for laser cleaning.

6.4.1.2 Surface Preparation of Lead Cathodes

Metals can also be coated on to the substrate *via* a variety of techniques, such as electroplating, evaporation, ion sputtering, or arc deposition. Although any metal can be deposited, lead coating has been tested for use in SCRF injectors (for example, at Helmholtz-Zentrum Berlin) and the process is presented here. Since arc deposition of lead was shown to deliver a higher QE than other techniques, it is being developed further. Figure 6.3 illustrates the arc-deposition system used for our measurements in three different configurations: Straight; 90° bend; and, 45° bend. We note that the left figure also shows the 1.3 GHz gun attached to the system in readiness for arc deposition. Figure 6.4 shows more details.

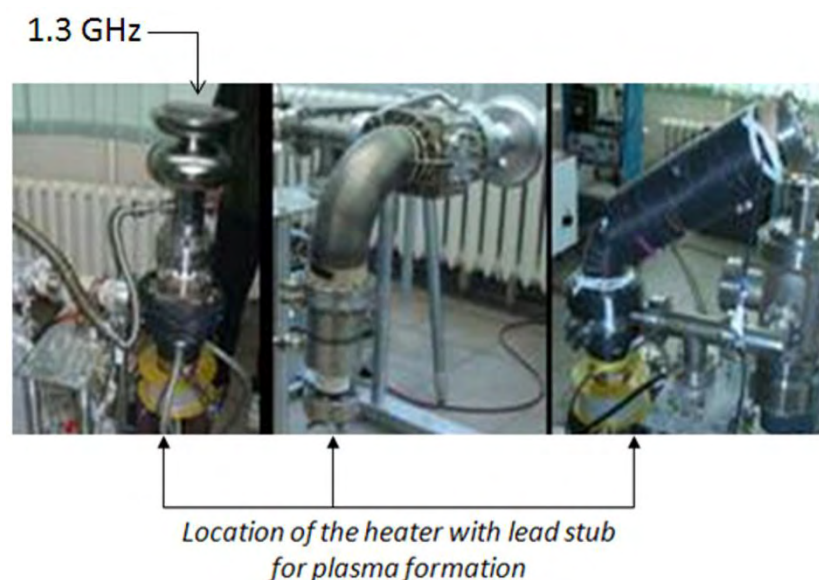


Figure 6.3. Arrangements for plasma arc deposition: Straight (left), 90° bend (center), and 45° bend (right).

In the arc-deposition system, a high-purity lead planar cathode is mounted on a water-cooled support inside a vacuum system capable of maintaining $< 10^{-11}$ Torr of pressure. The cathodic arc of lead is guided through a magnetic filter that removes micro-droplets from the arc, and deflects the stream of plasma ions towards the gun. A specially designed shield assures that the central portion of the cavity's back surface is coated with lead, while protecting the rest of the cavity. The gun is electrically isolated from the walls of the vacuum chamber and is either DC- or pulse- (kilohertz range) biased to 100 V. The lowest possible arc current for stable operation in the DC mode is ~ 23 A, whilst the upper limit is set to 140 A by the anode's

cooling system. The deposition rate depends on the distance between the cathode and the target, and is typically $\sim 0.5 \text{ nm s}^{-1}$. Additional details of the system are given elsewhere [6.21].

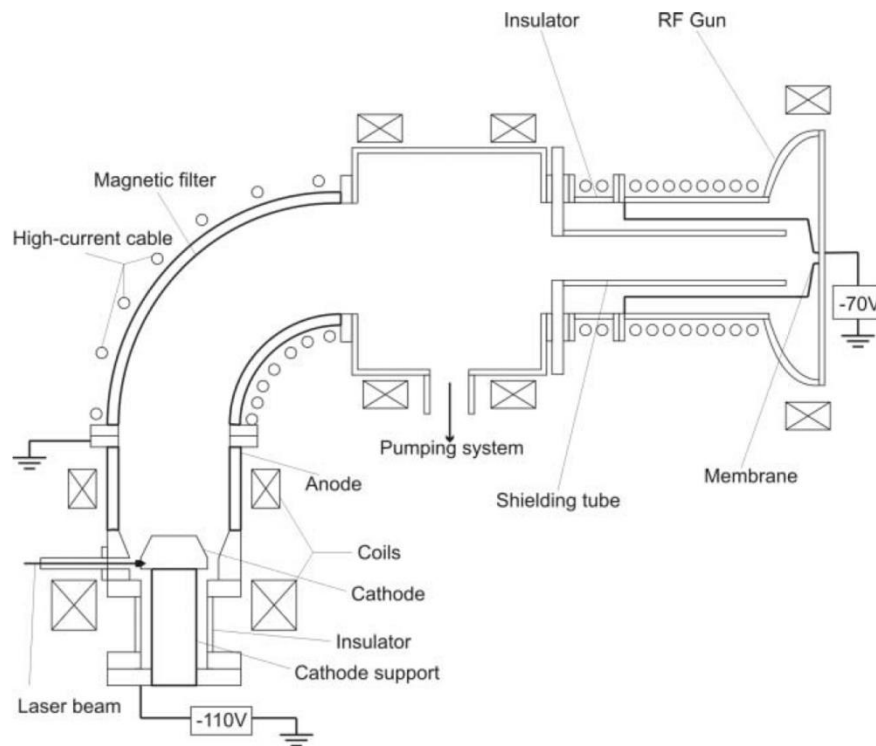


Figure 6.4. Details of the arc deposition system, with 1.3 GHz gun attached, for depositing lead. [[6.21]; Available under Creative Commons Attribution 3.0 License (www.creativecommons.org/licenses/by/3.0/us/) at www.JACoW.org.]

In the straight set-up, there is no magnetic filter, the spacing between the cathode and the target is shorter, and the resulting coating thicker (approximately micrometers) than in the other configurations. However, the surface contains droplets of lead, making the coating's thickness slightly non-uniform. With the 90° bend, the droplets were eliminated, but the coating thickness was limited to 100 nm, based on SEM EDS measurements. This thickness is not adequate to ensure the efficient absorption of photons, as well as effective laser cleaning. Although the QE of the 100 nm thick sample improved significantly with laser cleaning, it did not reach the highest value (0.5% @ 193 nm) of the original arc-deposited witness sample. The deposition parameters must be optimized to obtain a micrometer thick coating without droplet formation and minimum contamination. However, lead cathode has been deposited in 1.3 GHz guns with this technique without significant degradation of the gun's RF properties; they were used to generate electron beams [6.12].

6.4.2 In-Situ Preparation

6.4.2.1 Laser Cleaning

The laser cleaning typically is done when the cathode is mounted in the RF cavity and the system has been pumped and baked to achieve a base pressure of $\leq 10^{-10}$ Torr. The laser is raster-scanned multiple times over the emitting surface with the scan step much smaller than the size of the laser spot, thereby smoothing out any spatial variation in the laser energy density to result in uniform emission. The density of the laser energy depends on the metal being cleaned. Table 6.3 lists the metals cleaned in the RF gun, as well as the minimum energy density required to clean the surface so that the QE is increased almost to its maximum value while the surface finish is preserved. Scanning with higher energy density may engender slightly

higher QE, but will modify the surface morphology, which is undesirable in the injector. Laboratory measurements indicate that an excimer laser with a 248 nm wavelength and ~5 ns pulse duration is as effective as a 266 nm laser with a picosecond pulse duration. Since the injector facilities already are equipped with picosecond UV lasers, these are the lasers of choice for cleaning. However, the energy density required to clean the surface without altering the surface morphology for the sub-picosecond pulse duration must be reestablished for the cathode material.

Metal	Energy Density of Cleaning Laser [mJ mm^{-2}]
Copper	1
Magnesium	0.1
Niobium	0.6
Lead	0.2

Table 6.3. Laser energy densities to clean the metal surface to improve the QE without altering the surface finish.

In high average current injectors, the dark current from the cathode needs to be minimized since it poses a significant radiation risk. Experimental measurements with Pb coated Nb in all-superconducting cavity to generate 1 mA average current has shown [6.21] that laser cleaning reduces dark current and increases the onset field for field emission. This could be attributed to the removal of field emitter sites during laser cleaning.

6.4.2.2 Ion Cleaning

Hydrogen ion cleaning of copper has improved [6.18] the QE of OFC significantly, as shown in Figure 6.5. However, cleaning increased sensitivity to surface contaminants, and hence, it is not being used for routine operation of the injector.

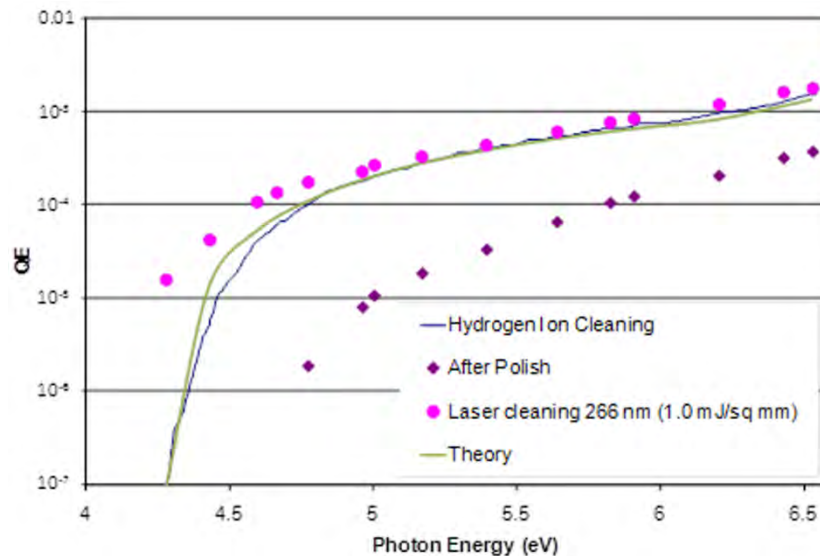


Figure 6.5. Comparison of LCLS copper cathodes before cleaning, after H-ion cleaning, and after laser cleaning. Both modes of cleaning resulted in an ultimate QE consistent with theoretical expectations.

6.5 IMPACT OF SURFACE FINISH ON EMITTANCE

The surface smoothness of the cathode may affect emittance in several ways. Any non-uniformity in the transverse profile of the cleaning laser can cause non-uniform electron emission, thereby degrading the

emittance. Hence, it is imperative to check the emitting surface carefully after laser cleaning to assure the uniformity of emission. Any surface roughness could lead to field enhancement and a corresponding reduction in the work function due to the Schottky effect. This also would lead to a non-uniform emission and degraded emittance as discussed in Chapter 5. Furthermore, the field bending associated with the field enhancement could entail larger transverse energy and a larger emittance of electrons. For applications sensitive to the transverse emittance, care must be taken to minimize these effects.

6.6 INCORPORATING THE CATHODE IN A GUN

NCRF injectors are usually made of OFC making it relatively easy to incorporate the copper cathode. However, the cleaning procedures required to attain a high QE from copper requires surface preparation that is not fully compatible with good RF performance. The same is true for the niobium cathode in SCRF guns. Different designs have been used for a de-mountable cathode; the successful ones are described below. In all cases, the critical issues are to preserve the quality of the RF field, eliminate high voltage breakdown, and maintain ultra-high vacuum (UHV) conditions.

6.6.1 Plug

The plug arrangement used in the early operation of BNL-ATF's injector is shown in Figure 6.6. A helical flex was used for the RF contact and metal gaskets to preserve the integrity of the vacuum. Figure 6.6(a) shows the helical flex and the pitting developed over time, caused by electrical breakdown in this region. Spring fingers also will achieve good RF contact, but they were found to cause greater electrical breakdown and associated pitting. The square pattern in Figure 6.6(b) depicts the result of laser cleaning. The entire plug can be made of the copper, incorporating the cathode, or a different material can be inserted at the center of the plug. An embedded magnesium cathode is illustrated in Figure 6.6(c). The four alignment fiducials in Figure 6.6(c) help in centering the laser spot on the cathode.

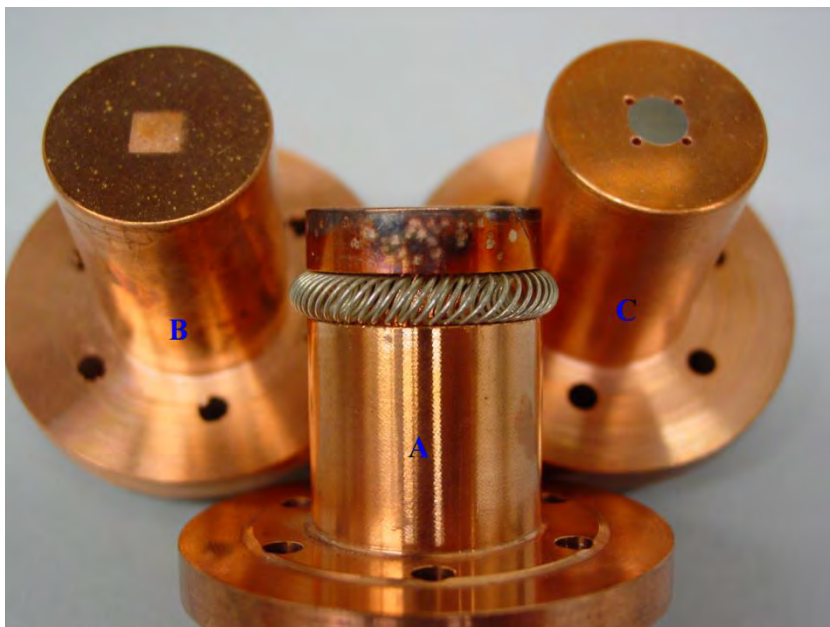


Figure 6.6. Photograph of plug cathodes tested at BNL-ATF. (a) Copper cathode with helical flex; (b) Surface of the plug showing the laser-cleaned area; and, (c) Copper plug with magnesium cathode.

Similar plug design also was used in the SCRF gun [6.23]. The niobium plug is pressure-fitted with an indium wire seal on the outside of the cavity. We also coated the Nb plug with lead and tested it in the same

arrangement. Since the heat load and associated degradation of the cavity, Q , are of serious concern for SCRF injectors, its design must address the effective cooling of the plug.

6.6.2 Flange Cathode

To avoid the breakdown problems encountered in the plug design, in later designs of NCRF injectors, the entire back plane of the cavity was replaced by a flange containing the cathode. Figure 6.7 shows examples of this design.

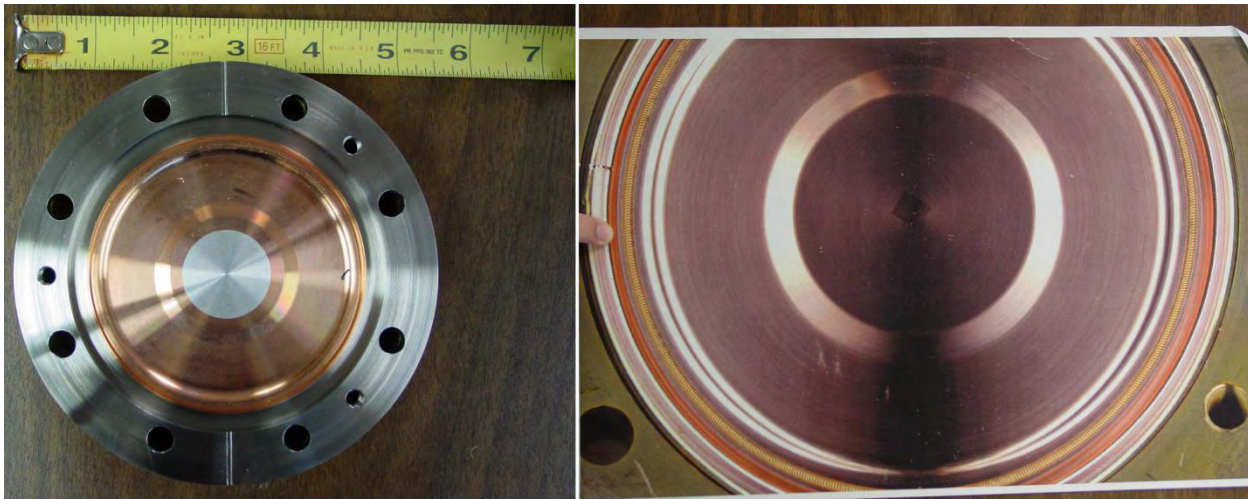


Figure 6.7. Flange cathode. Left: Magnesium friction-welded to the copper flange. Right: Copper cathode. The square in the center is due to laser cleaning. In both cases, a helical flex is used for RF contact and gaskets to preserve the vacuum's integrity.

The magnesium cathode, shown in left photograph of Figure 6.7, is friction-welded to the flange. Figure 6.8 illustrates a cross-section of this friction-welded region.



Figure 6.8. Cross section of magnesium friction-welded flange.

As evident in Figure 6.8, the top surface of the magnesium is slightly higher than the back-plate, which was reduced and polished using the procedure described in Section 6.3.1.1. To avoid trapping gases, friction welding can be carried out under vacuum.

6.6.3 Choke Joint

Another method of integrating the cathode in a gun, especially in an SCRF gun, is using a choke joint. The cathode material is held in a separate support structure, thermally, and electrically isolated from the cavity; it can be kept at a temperature higher than the cavity and cooled by liquid nitrogen instead of helium. The coaxial line formed by the cathode's channel and its stalk would lead to RF power leakage, which is minimized by using a carefully designed filter. The Cs_2Te cathode was successfully tested with such a gun at the Forschungszentrum Dresden-Rossendorf (FZD laboratory [6.23]–[6.26]). This scheme, as shown in Figure 6.9, advantageously incorporates a demountable cathode, a requirement for guns using sensitive, short-lifetime cathodes while preserving the cryogenic temperature of the SCRF cavity.

Furthermore, this arrangement facilitates testing different types of cathodes in the same gun, supporting a one-to-one comparison. Power leakage also is ameliorated by incorporating a RF choke joint in the cavity. The design of the choke joint is non-trivial; multipacting could cause problems if the gun is operating at high accelerating fields [6.27]. Several approaches can resolve this issue, such as incorporating a groove to change the trajectory of the multipacting electrons, biasing the stalk to repel them, and coating the surface with a low-yield material.

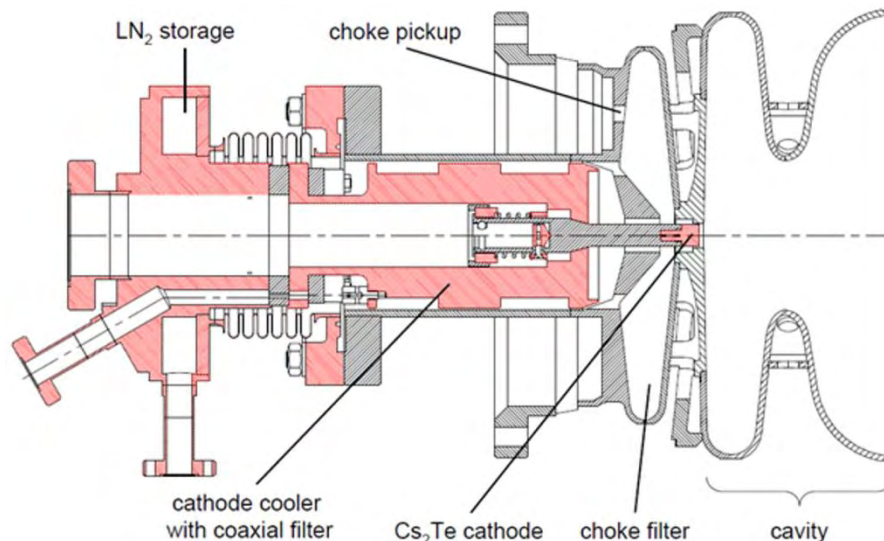


Figure 6.9. Schematic of the choke joint used in SCRF gun. [6.28]; Courtesy of A. Arnold, Helmholtz-Zentrum Dresden Rossendorf, Institut für Strahlenphysik, Strahlungsquelle ELBE (FWKE)]

6.7 CONCLUSION

We described in this chapter the relative merits and drawbacks of methods that currently are used to prepare metal photocathodes, to improve their electron yield, and to incorporate them into the injector. This field is still evolving, and the focus is on encompassing the physics behind the processes as well as the processes themselves. We anticipate that the next decade will bring better understanding and new and improved cathodes.

6.8 CONFLICT OF INTEREST AND ACKNOWLEDGEMENT

We confirm that this article content has no conflicts of interest and would like to acknowledge the support of the US Department of Energy under contract numbers DOE DE-SC0003965 and DE-AC02-98CH10886.

References

- [6.1] K. Batchelor, I. Ben-Zvi, R. C. Fernow *et al.*, “Performance of the Brookhaven photocathode RF gun”, *Nucl. Instrum. Meth. A*, vol. 318, pp. 372-376, July 1992.
- [6.2] J. Rosenzweig, K. Bishofberger, X. Ding *et al.*, “The Neptune photoinjector”, *Nucl. Instrum. Meth. A*, vol. 410, pp. 437-451, June 1998.
- [6.3] X. J. Wang, T. Srinivasan, K. Batchelor *et al.*, “Photoelectron beam measurements for Mg cathode in a RF electron gun”, in *16th Int. Free Electron Laser Conf.*, 1994, pp. 21-26.
- [6.4] D. H. Dowell, E. Jongewaard, C. Limborg-Deprey *et al.*, “Results of the SLAC LCLS gun high-power RF tests”, in *Proc. 2007 Particle Accelerator Conf.*, 2007, pp. 1296-1298.
- [6.5] T. Rao, “Updates from facilities: ANL, BNL, Cornell, JLAB, LBNL, European Labs, Japanese Labs”, presented at Workshop Photocathode Physics Photoinjectors, Brookhaven National Laboratory, October 2010.
- [6.6] J. Sekutowicz, I. Ben-Zvi, J. Rose *et al.*, “Proposed continuous wave energy recovery operation of an X-ray free electron laser”, *Phys. Rev. ST Accel. Beams*, vol. 8, 010701-1–010701-12, January 2005.
- [6.7] I. Ben-Zvi, D. Barton, D. Beavis *et al.*, “Extremely high current, high-brightness energy recovery linac”, in *Proc. 2005 Particle Accelerator Conf.*, 2005, pp. 1150-1152.
- [6.8] I. Ben-Zvi, V. Litvinenko, D. Barton *et al.*, “Electron cooling of RHIC”, in *Proc. 2005 Particle Accelerator Conf.*, 2005, pp. 2741-2743.
- [6.9] T. Rao, I. Ben-Zvi, A. Burrill *et al.*, “Design, construction and performance of all niobium superconducting radio frequency electron injector”, *Nucl. Instrum. Meth. A*, vol. 562, pp. 22-33, June 2006.
- [6.10] J. Smedley, T. Rao and Q. Zhao, “Photoemission studies on niobium for superconducting photoinjectors” *J. Appl. Physics*, vol. 98, pp. 043111-1–043111-6, August 2005.
- [6.11] J. Smedley, T. Rao and J. Sekutowicz, “Lead photocathodes”, *Phys. Rev. ST Accel. Beams*, vol. 11, 013502-1–013502-9, January 2008.
- [6.12] J. Smedley, Rao, T. Kneisel, P. *et al.*, “Photoemission tests of a Pb/Nb superconducting photoinjector”, in *Proc. 2007 Particle Accelerator Conf.*, 2007, pp. 1365-1367.
- [6.13] T. Srinivasan-Rao, J. Fischer and T. Tsang, “Photoemission studies on metals using picosecond ultraviolet laser pulses”, *J. Appl. Physics*, vol. 69, pp. 3291-3296, March 1991.
- [6.14] C. N. Berglund and W. E. Spicer, “Photoemission studies on copper and silver: theory”, *Phys. Rev.*, vol. 136, pp. A1030-A1044, November 1964.
- [6.15] T. Ogata, Computational Electronic Structure Database. Available Online: <http://mits.nims.go.jp/matnavi/> [Accessed: January 30, 2012].
- [6.16] C. Norris and L. Walldén, “Photoemissions from Pb”, *J. Physics F: Metal Physics*, vol. 2, pp. 180-188, January 1972.
- [6.17] H. G. Liljenvall, A. G. Mathewson and H. P. Myers, “The optical properties of lead in the energy range 0.6-6 eV”, *Philosph. Mag.*, vol. 22, pp. 243, 1970.
- [6.18] D. H. Dowell, F. K. King, R. E. Kirby *et al.*, “*In Situ* cleaning of metal cathodes using a hydrogen ion beam”, *Phys. Rev. ST Accel. Beams*, vol. 9, pp. 063502-1–063502-8, June 2006.
- [6.19] C. P. Hauri, R. Ganter, F. Le Pimpec *et al.*, “Intrinsic emittance reduction of an electron beam from metal photocathodes,” *Phys. Rev. Lett.*, vol. 104, pp. 234802-1–234802-4, June 2010.
- [6.20] H. J. Qian, C. Li, Y. C. Du *et al.*, “Experimental investigation of thermal emittance components of copper photocathode,” *Phys. Rev. ST Accel. Beams*, vol. 15, pp. 04012-1–04012-8, April 2012.
- [6.21] P. Strzyzewski, L. Langner, M. J. Sadowski *et al.*, “Deposition of lead thin films used as photocathodes by means of cathodic arc under UHV conditions”, in *Proc. 2006 European Particle Accelerator Conf.*, 2006, pp. 3209-3211.

- [6.22] A. Neumann, W. Anders, R. Barday *et al.*, “First characterization of a fully superconducting RF photoinjector cavity,” in *Proc. 2011 Int. Particle Accelerator Conf.*, 2011, pp. 41-43.
- [6.23] P. Kneisel, J. Sekutowicz, R. Lefferts *et al.*, “Preliminary results from a superconducting photocathode sample cavity”, in *Proc. 2005 Particle Accelerator Conf.*, 2005, pp. 2956-2958.
- [6.24] D. Janssen, H. Büttig, P. Evtushenko *et al.*, “First operation of a superconducting RF-gun”, *Nucl. Instrum. Meth. A*, vol. 507, pp. 314-317, July 2003.
- [6.25] A. Arnold, H. Büttig, D. Janssen *et al.*, “Development of a superconducting radio frequency photoelectron injector”, *Nucl. Instrum. Meth. A*, vol. 577, pp. 440-454, July 2007.
- [6.26] P. Murcek, A. Arnold, H. Buettig *et al.*, “Modified 3½-cell SC cavity made of large grain niobium for the FZD SRF injector”, in *Proc. 2009 Superconducting RF Conf.*, 2009, pp. 585-588.
- [6.27] A. Burrill, I. Ben-Zvi, M. Cole *et al.*, “Multipacting analysis of a quarter wave choke joint used for insertion of a demountable cathode into a SRF photoinjector”, in *Proc. 2007 Particle Accelerator Conf.*, 2007, pp. 2544-2546.
- [6.28] André Arnold, private communication, 2011.